Fronts, domain growth, and dynamical scaling in a $d=1$ nonpotential system

R. Gallego, M. San Miguel, and R. Toral
Instituto Mediterráneo de Estudios Avanzados, Consejo Superior de Investigaciones Científicas, Universitat de les Illes Balears, E-07071 Palma de Mallorca, Spain*
(Received 17 November 1997; revised manuscript 6 April 1998)

By considering the inclusion of nonpotential terms in a model system that has the basic symmetries of a $n=3$ clock model, we study the issues of dynamical scaling, front motion, and domain growth in a one-dimensional nonpotential situation. For such a system without a Lyapunov potential, the evolution follows a nonrelaxational dynamics with the consequence that fronts between otherwise equivalent homogeneous states move at a velocity dictated by the strength δ of the nonpotential terms and the asymptotic state can no longer be associated with a final equilibrium state. In fact, for large enough δ, the system undergoes a transition towards a situation of spatiotemporal chaos that is in many aspects equivalent to the Küppers-Lortz instability for Rayleigh-Bénard convection in a rotating cell. We have focused on the transient dynamics below this instability, where the evolution is still nonrelaxational and the dynamics is dominated by front motion. We classify the families of fronts and calculate their shape and velocity. We deduce that the growth law for the domain size is nearly logarithmic with time for short times and becomes linear after a crossover, whose width is determined by the value of δ. This prediction is validated by numerical simulations that also indicate that a scaling description in terms of the characteristic domain size is still valid as in the potential case.
[S1063-651X(98)04809-0]

PACS number(s): 47.20.−k, 47.54.+r, 05.70.Ln

I. INTRODUCTION

A noteworthy result in the study of nonequilibrium statistical mechanics is the existence of dynamical scaling during the coarsening process in which a system approaches equilibrium after undergoing a phase transition [1,2]. Dynamical scaling reflects that domain growth is self-similar with a single time dependent characteristic length. In the simplest case of a relaxational dynamics for a scalar order parameter, which models, for example, an order-disorder transition (model A in the taxonomy of [3]), domains of two equivalent phases grow locally from an unstable state, and the approach to a final equilibrium state is dominated by interface motion. For spatial dimension $d>1$, the mechanism for domain growth is curvature driven interface motion. This leads to a characteristic length growing as $R\sim t^{1/2}$. This type of phenomenon has been studied in a large variety of systems that share the common feature that the final state of the dynamics is a state of thermodynamic equilibrium, which minimizes a free energy or ''potential'' of the problem. Transient dynamics might also include additional processes beyond pure relaxation in that potential [4,5], but a measure of relative stability between stationary states is guaranteed by the existence of the potential. A more genuine nonequilibrium dynamics occurs when such a potential does not exist. A natural question, which we address in this paper, is the existence of dynamical scaling in the approach to a final stationary state that does not follow the minimization of a potential, while this transient dynamics from an unstable state involves the formation of spatial domains. A numerical study of domain coarsening in a nonpotential dynamics was reported in Ref. [6]. The question of dynamical scaling can also be addressed for Hamiltonian dynamics [7], which is the extreme opposite situation to that of dissipative relaxational dynamics in a potential. A general nonequilibrium situation will, in general, have contributions from both types of dynamics [4,5].

The motion of an interface between two linearly stable solutions of a dynamical system was long ago proposed as a measure of relative stability for a nonpotential system [8], and the motion of interfaces, domain walls, or front solutions has been studied in a number of nonpotential systems [9–12]. It is known that a domain wall between two equivalent states with different broken symmetry can move in $d=1$ in either direction due to nonpotential dynamics [9]. Likewise, nonpotential dynamics can stabilize front solutions that, in the potential limit, would move from a globally stable into a metastable state [11]. It is the purpose of this paper to study the consequences of interface motion driven by nonpotential dynamics on coarsening processes and dynamical scaling, which by and large have not been considered.

To this end, and as a first step towards understanding the problem of domain growth and dynamical scaling in nonrelaxational systems, we consider the addition of specific nonpotential terms to the one dimensional three-component vector model of statistical mechanics [13] (a field model that has the basic symmetries of the $q=3$ Potts or the $n=3$ clock models) describing three competing, nonconserved order parameters with short-range self-interactions. It turns out that the new nonpotential terms imply that the zero-dimensional version of the resulting model is analogous to the Busse-Heikes model for Rayleigh-Bénard convection in a rotating cell and also mathematically equivalent to the May-Leonard biological model of competition between three species. Although the model studied here is not a realistic model for Rayleigh-Bénard convection in a rotating cell [14], one can still use the analogy to get an intuitive physical interpretation of the dynamical evolution of the system. It is known that, for the fluid system, and beyond a threshold value for the

*URL: http://www.imedea.uib.es/PhysDept

parameter, δ, measuring the strength of the nonpotential terms (related to the rotation speed of the cell) an instability to a time dependent dynamics occurs (Küppers-Lortz instability [15,16]). Below this instability, but still taking the system beyond the Rayleigh-Bénard convective instability, locally ordered domains, associated with different orientations of the convective rolls, emerge. The subsequent coarsening process seems to be stopped by the Küppers-Lortz instability in $d=2$ [17,18]. However, below the instability to a time dependent state, three preferred orientations exist and the motion of interfaces separating them is subject to nonpotential dynamics that will affect domain growth.

Another reason for using this system is that dynamical scaling in $d=1$ potential systems is a special case for which well established results are available [2,19]: for the simplest case of a scalar nonconserved order parameter with short range interactions, a scaling solution is known with a logarithmic growth law for the typical domain size, $R\sim \ln t$ [20,21]. This regime follows an early time regime of domain formation with a growth law $R\sim t^{1/2}$ [22]. The logarithmic domain growth has its origin in the interactions between domain walls [23]. The velocity of domain wall motion in these circumstances can be calculated by a perturbation analysis [10]. We study how these results are modified by nonpotential dynamics. We find that dynamical scaling still holds, but with a crossover between two well defined regimes characterized by a logarithmic and linear domain growth law, respectively. The two growth laws can be traced back to the two mechanisms that determine domain wall motion. The first one is the interaction between domain walls as in the potential case. The second one is due to the fact that the nonpotential dynamics causes isolated individual fronts to move with finite velocity. In a multifront configuration this provides an additional coarsening mechanism in which fronts moving in opposite directions annihilate each other. The crossover time between the two dominant mechanisms described depends on the strength of nonpotential terms. When these become large enough, the logarithmic regime is pushed to just the very early times. In this case finite size effects become also important since very large domains emerge rather fast.

The outline of the paper is as follows: in Sec. II we introduce the nonpotential model and describe its homogeneous stationary solutions. In Sec. III we classify nonhomogeneous front solutions and compute their velocity. We also analyze the interactions between two fronts including the nonpotential effects. In Sec. IV we discuss the issue of dynamical scaling and the growth law. We present numerical simulations that show the validity of the dynamical scaling description when nonpotential terms are present. Finally, in Sec. V we end with some conclusions and an outlook.

II. THEORETICAL MODEL

We base our theoretical approach on the following model:

$$\partial_t A_i = -\frac{\delta \mathcal{F}}{\delta A_i} - \delta f_i, \quad i=1,2,3. \tag{2.1}$$

Here A_1, A_2, and A_3 are real scalar fields. For the potential function $\mathcal{F}$ we choose that of the well-known $n=3$ vector model [13]:

$$\mathcal{F}[A_1,A_2,A_3]=\int dx\left\{\frac{1}{2}\sum_{i=1}^{3}(\partial_x A_i)^2+\frac{\eta}{2}\Phi^2-\frac{1}{2}\Phi-\frac{\eta-1}{4}\Psi\right\}, \tag{2.2}$$

where $\Phi=\Sigma_{i=1}^{3}A_i^2$ and $\Psi=\Sigma_{i=1}^{3}A_i^4$. The nonpotential terms are chosen as

$$\begin{aligned} f_1&=A_1(A_2^2-A_3^2),\\ f_2&=A_2(A_3^2-A_1^2),\\ f_3&=A_3(A_1^2-A_2^2). \end{aligned} \tag{2.3}$$

In the case $\delta=0$ the dynamical flow is of a *relaxational gradient* type [4,5], that is, there exists a Lyapunov functional ($\mathcal{F}$) that monotonically decreases in time. When $\delta\neq 0$, however, one cannot find generally such a functional and we say that the system is *nonpotential*.

The resulting equations of motion are

$$\begin{aligned} \partial_t A_1&=\partial_x^2 A_1+A_1[1-A_1^2-(\eta+\delta)A_2^2-(\eta-\delta)A_3^2],\\ \partial_t A_2&=\partial_x^2 A_2+A_2[1-A_2^2-(\eta+\delta)A_3^2-(\eta-\delta)A_1^2],\\ \partial_t A_3&=\partial_x^2 A_3+A_3[1-A_3^2-(\eta+\delta)A_1^2-(\eta-\delta)A_2^2], \end{aligned} \tag{2.4}$$

and they form the basis of our subsequent analysis. Notice that the system is invariant under the following transformations:

(a) $x\to x+x_0$, $t\to t+t_0$ (spatio-temporal translation symmetry),

(b) $A_1\to A_2, A_2\to A_3$, $A_3\to A_1$ (cyclic permutation symmetry),

(c) $A_i \rightleftarrows A_j$, $\delta\to-\delta$, where A_i, A_j are any two different amplitudes.

The previous analysis shows that A_1, A_2, and A_3 are ''equivalent'' variables (from the dynamical point of view).

A similar set of equations is introduced in Ref. [24] for some particular values of the parameters η, δ in the context of population dynamics. In their case A_i^2 represents the population of a biological species.

If one neglects the spatial dependence of the fields A_i we recover a model first proposed in the context of fluid dynamics by Busse and Heikes [16], which is mathematically equivalent to a model of three competing biological species [25]. In the Busse-Heikes model, A_1, A_2, and A_3 are the amplitudes of the three selected modes corresponding to three different orientations of the convection rolls in the rotating cell. For this fluid case, δ is related to the rotation speed such that $\delta=0$ is the nonrotating case; the parameter η is related to other fluid properties. The analysis of [16] and [25] shows that, for a certain range of the parameters η and δ (see next section), there are no homogeneous stable solutions and the dynamics tends asymptotically to a sequence of alternations of the three modes. An unwanted feature of the previous model is that the alternation time is not constant, but increases with time, contrary to experiments where an approximately constant period is observed. Busse and Heikes

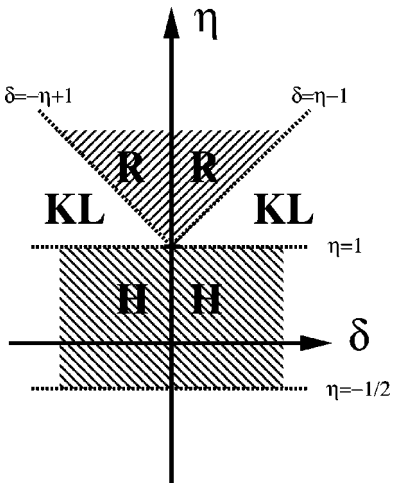

FIG. 1. Linear stability diagram of the homogeneous solutions of Eq. (2.4). Inside the region labeled R, rolls are stable whereas in the H region, the stable solution is the hexagon. The KL region corresponds to the Küppers-Lortz instability.

proposed that the addition of small noise could stabilize the period [5,26], but an alternative explanation considered the addition of space-dependent terms to the equations. Although the symmetries that must satisfy the amplitude equations would imply that the spatially dependent terms should be of a specific form [27–29], it has been shown in [17] that these can be further simplified without altering the essentials of the problem. Our one dimensional model with equivalent space-dependent terms for the three variables does not satisfy the proper symmetries holding in the fluid case. However, it is still true that we can use the fluid analogy to gain some insight into the dynamical behavior of the model. For this reason we will refer often to the A_i's as the ''amplitude'' fields.

There exist two kinds of homogeneous solutions that are stable in some region of the parameter space spanned by η and δ. These are three ''roll'' solutions $A_i=1$, $A_j=0$ $(j\neq i)$, $i=1,2,3$, and one ''hexagon'' solution $A_1=A_2=A_3=1/\sqrt{1+2\eta}$ (this solution requires $\eta>-1/2$). A linear stability diagram of these solutions is shown in Fig. 1. We have focused on the region labeled with the letter R for values of δ below the Küppers-Lortz instability $(|\delta|<\eta-1)$ and where the rolls are the stable solutions. In this region we expect the formation of domain walls connecting homogeneous stable roll solutions.

III. FRONT SOLUTIONS

A. Isolated fronts

In the context of the present study, fronts or domain walls are defects that connect two stable homogeneous solutions. Fronts in one dimension are usually termed *kinks* and we will often refer to them in this way. We focus on the space-dependent stationary solutions of Eq. (2.4) with $\delta=0$. The stable kink solutions are such that one of the three amplitudes, say A_k, satisfying the boundary conditions $A_k(x\to\pm\infty)=0$, is zero everywhere. In order to study the dynamics of the nonpotential kinks, we first consider the kinks associated with the stationary potential problem and then we treat the nonpotential terms as a perturbation. The two nonvanishing stationary amplitudes A_i and A_j are, for $\delta=0$, solutions of

$$\begin{aligned}\partial_x^2 A_i &= -A_i+A_i^3+\eta A_i A_j^2,\\ \partial_x^2 A_j &= -A_j+A_j^3+\eta A_j A_i^2,\end{aligned} \tag{3.1}$$

with boundary conditions $A_i(-\infty)=A_j(+\infty)=0$ and $A_i(+\infty)=A_j(-\infty)=1$.

The system (3.1) may be considered to represent the two dimensional motion of a Newtonian particle of unit mass $(x\to t,\ A_i\to X,\ A_j\to Y)$ under the action of a force with potential function $V(X,Y)=\frac{1}{2}(X^2+Y^2)-\frac{1}{4}(X^4+Y^4)-\frac{1}{2}\eta X^2Y^2$. This function has two maxima in $m_0=\{A_i=1,A_j=0\}$ and $m_1=\{A_i=1,A_j=1\}$. It is clear that there exists a unique trajectory (allowed by the dynamics) along which a particle located in $m_0(m_1)$ can reach $m_1(m_0)$. The kink profile corresponds to the variation in time of the particle coordinates $(X(t),Y(t))$ when it moves between the two maxima [30].

An explicit analytical solution can be found in two particular cases [31]. First, when $0<\eta-1\ll 1$, we have

$$\begin{aligned}A_i^0(x) &= r(x)[1+\exp(2\sqrt{\eta-1}(x-x_0))]^{-1/2},\\ A_j^0(x) &= r(x)\ e^x[1+\exp(2\sqrt{\eta-1}(x-x_0))]^{-1/2},\end{aligned} \tag{3.2}$$

with $r(x)=1+(\eta-1)R(x)$, $R(x)=O(1)$. Secondly, when $\eta=3$ it is possible to obtain exact analytical solutions:

$$\begin{aligned}A_i^0(x) &= \frac{1}{1+e^{\mp\sqrt{2}(x-x_0)}}=\frac{1}{2}\left[1\pm\tanh\left(\frac{x-x_0}{\sqrt{2}}\right)\right],\\ A_j^0(x) &= \frac{1}{1+e^{\pm\sqrt{2}(x-x_0)}}=\frac{1}{2}\left[1\mp\tanh\left(\frac{x-x_0}{\sqrt{2}}\right)\right].\end{aligned} \tag{3.3}$$

In both cases x_0 is arbitrary but fixed. From these solutions it is clear that the spatial scale over which A_i^0 and A_j^0 vary is of order $1/\sqrt{\eta-1}$.

The three roll solutions are equivalent and they yield the same value for the Lyapunov functional (2.2). Therefore, we expect isolated kinks not to move in the potential problem $(\delta=0)$. We now ask about the persistence of these kink solutions when δ is different from zero. For this we will use singular perturbation theory. Let us assume δ to be small, say of order ε, and look for a solution of Eq. (2.4) [with $A_k(x)=0$] of the form

$$\begin{aligned}A_i(x) &= A_i^0(x-s(t))+\varepsilon\ A_i^1(x-s(t))+O(\varepsilon^2),\\ A_j(x) &= A_j^0(x-s(t))+\varepsilon\ A_j^1(x-s(t))+O(\varepsilon^2),\end{aligned} \tag{3.4}$$

where $A_i^0(x)$ and $A_j^0(x)$ are solutions of Eq. (3.1). Substituting into Eq. (2.4) and matching the terms of the same order in ε, we find, at order $O(\varepsilon^0)$,

$$\begin{aligned}\partial_x^2 A_i^0+A_i^0-(A_i^0)^3-\eta A_i^0(A_j^0)^2=0,\\ \partial_x^2 A_j^0+A_j^0-(A_j^0)^3-\eta A_j^0(A_i^0)^2=0,\end{aligned} \tag{3.5}$$

and at order $O(\varepsilon^1)$

$$\mathcal{L}\boldsymbol{\alpha}=\boldsymbol{\alpha}', \tag{3.6}$$

where

$$\mathcal{L}=\begin{pmatrix} \partial_x^2+1-\eta[(A_i^0)^2+(A_j^0)^2] & -2\eta A_i^0 A_j^0 \\ -2\eta A_i^0 A_j^0 & \partial_x^2+1-\eta[(A_i^0)^2+(A_j^0)^2] \end{pmatrix},$$

$$\boldsymbol{\alpha}=\begin{pmatrix} A_i^1 \\ A_j^1 \end{pmatrix}, \quad \boldsymbol{\alpha}'=\begin{pmatrix} \delta\varepsilon^{-1}(A_i^0)^2 A_j^0 - A_i^0\partial_t s \\ -\delta\varepsilon^{-1}A_j^0(A_i^0)^2 - A_j^0\partial_t s \end{pmatrix}.$$

The solvability condition for the existence of a solution $[A_i^1(x),\ A_j^1(x)]$ reads

$$(\boldsymbol{\Phi}^\dagger,\ \boldsymbol{\alpha}')=0, \tag{3.7}$$

where $(\cdot,\cdot)$ is a scalar product in $L^2(\mathbb{R})$ defined by $(f,g)=\int_{-\infty}^{\infty}dx f(x)^* g(x)$ and $\boldsymbol{\Phi}^\dagger$ belongs to the null space of the autoadjoint operator $\mathcal{L}$. Because of the translational invariance, $\mathcal{L}$ has a zero eigenvalue so that its kernel is not empty. The associated eigenvector is

$$\boldsymbol{\Phi}^\dagger=\begin{pmatrix} \partial_x A_i^0 \\ \partial_x A_j^0 \end{pmatrix}. \tag{3.8}$$

This is immediately seen taking, for example, the derivative of Eq. (3.5) with respect to x. Equation (3.7) can now be explicitly evaluated. From this equation, the solitary *kink velocity* in the nonpotential case is obtained at leading order:

$$v(\delta)\equiv\partial_t s=\delta\frac{\int_{-\infty}^{\infty}dx\ A_i^0 A_j^0(A_j^0\partial_x A_i^0 - A_i^0\partial_x A_j^0)}{\int_{-\infty}^{\infty}dx[(\partial_x A_i^0)^2+(\partial_x A_j^0)^2]}+O(\delta^2). \tag{3.9}$$

Therefore, in the nonpotential case, the kink moves despite connecting states associated with the same value of the Lyapunov potential of the equilibrium problem, as already known for other problems [9]. For the particular case of $\eta=3$ for which an analytical result is available for the kink profile [Eq. (3.3)], an explicit result is obtained for the solitary kink velocity, namely, $v(\delta)=\delta\sqrt{2}/4$.

The expression (3.9) gives not only the magnitude of the velocity but also the direction of motion, which is related to the sign of v. First, we note that the velocity is at leading order proportional to δ, so the direction of the motion depends upon the sign of δ. To illustrate how Eq. (3.9) determines the direction, let us consider, for example, a kink with boundary conditions: $A_i(-\infty)=A_j(+\infty)=0$ and $A_i(+\infty)=A_j(-\infty)=1$; $A_i^0(x)$ and $A_j^0(x)$ are such that $\partial_x A_i^0>0$ and $\partial_x A_j^0<0$. In this case the numerator of Eq. (3.9) is positive and v has the sign of δ. A positive (negative) value of v corresponds to a kink moving to the right (left). In Fig. 2 we show a classification of the six possible types of isolated kinks and their direction of motion. Three of them move in one direction and the other three in the opposite direction.

We have checked numerically the domain of validity of the perturbative result (3.9) (see Fig. 3). To check Eq. (3.9) we either use the analytical result of the kink profile A_i^0 for $\eta=3$, or, more generally, the kink profile A_i^0 obtained numerically. For a value of $\eta=3.5$, we see that the perturbative result to first order in δ, Eq. (3.9), turns out to be in good agreement with the numerical results approximately for values of $\delta\lesssim 1.5$. Of course this upper limit of validity depends on η in such way that it gets bigger as η is larger. Above this limit the linear relation between v and δ is no longer valid and one needs to compute further corrections in terms of successive powers of δ.

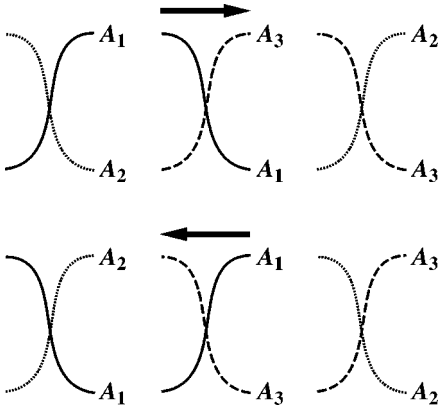

FIG. 2. Kinds of fronts and their direction of motion for $\delta>0$. The remaining amplitude for each kink is understood to be zero across the interface. For $\delta<0$ the picture is the same but with the arrows interchanged.

B. Multifront configurations

To study transient dynamics and domain growth we consider random initial conditions of small amplitude around the unstable solution $A_1=A_2=A_3=0$. In this situation a multifront pattern emerges rather than a solitary kink. In order to study dynamical scaling, we are interested in the late stage of this dynamics, once well-defined domains have been formed.

In a potential system governed by a nonconserved scalar order parameter with short-range interactions, as is the case with $\delta=0$, late time dynamics can be explained in terms of the interaction (and further annihilation) among adjacent kinks [24,20,21,23]. An isolated kink is stable. The interacting force between kinks turns out to be proportional to $\exp(-\alpha d)$ [23], where α is some *positive* constant related to the interface width and other system parameters, and d is the

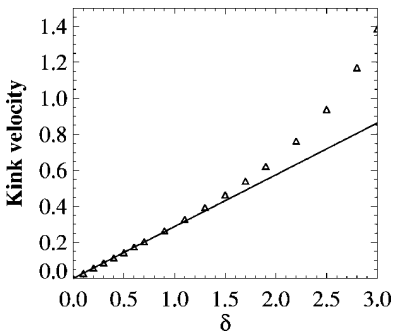

FIG. 3. Solitary kink velocity as a function of the nonpotential parameter δ for $\eta=3.5$. The straight line corresponds to the theoretical perturbative approach (3.9) whereas the points come from numerical simulation. Here and in the remaining figures, magnitudes are in the dimensionless units of Eq. (2.4).

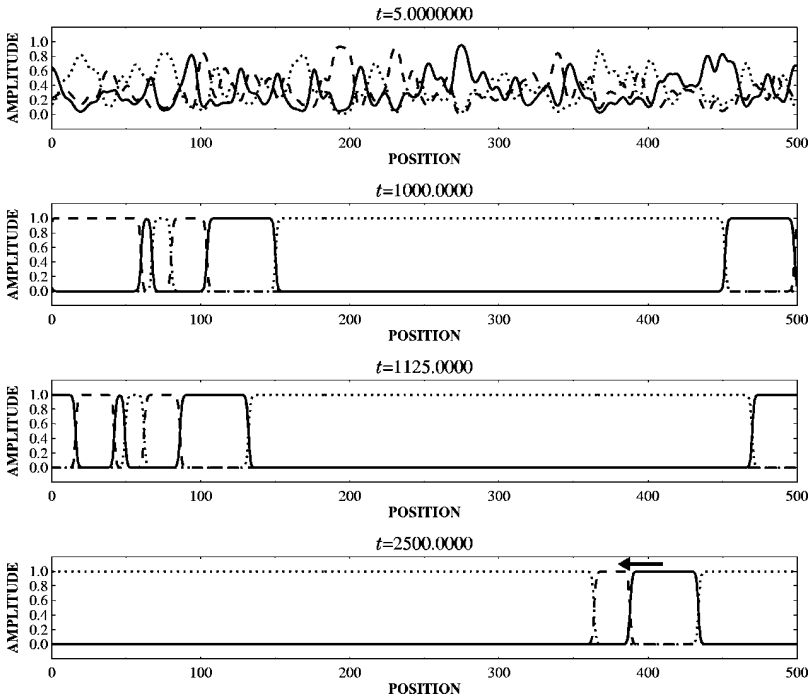

FIG. 4. Snapshots of the temporal evolution of the system. Parameter values: $\eta=3.5$, $\delta=0.5$, $L=500$.

distance between two adjacent kinks. This interaction among kinks leads to a growth law for the characteristic length that depends on time logarithmically [20,21]. The force is attractive and leads to kink annihilation. The process occurs in such a way that the domain that vanishes first is the smallest one. Kink annihilation occurs in a very small time scale. In fact, the hypothesis of ''instantaneous annihilation'' has been found to be a good assumption [20]. Kink annihilation induces domain coarsening, leading to a final state with a homogeneous roll solution filling up the whole system.

When δ is different from zero the long stage dynamics should still be explained in terms of moving fronts that annihilate each other. But now two very distinct competing physical phenomena come into play. On the one hand, there is the aforementioned kink interaction. On the other hand, we have the kink motion driven by nonpotential effects. In this case, we do not expect the growth law to be logarithmic, at least in the regime where the nonpotential effects (the strength of which is measured by δ) are important. In Fig. 4 we show some snapshots corresponding to a typical run of the temporal evolution of the system (we use periodic boundary conditions). The first snapshot corresponds to an early stage during which domains are forming. Once formed, kinks move in such a way that annihilations of contrapropagating adjacent kinks leads to coarsening. Eventually, as corresponding to the last snapshot, the system may be in a state with a group of kinks moving all in the same direction. These will interact among them (with an interaction force that varies logarithmically with the interkink distance) until extinction.

We have performed a perturbation analysis of domain growth in the simplest example of a single domain bounded by two moving domain walls. A differential equation for the domain size $s(t)$ can be obtained in the general case (see Appendix). For $\eta=3$ it adopts the simple form

$$\partial_t s(t)=2v(\delta)-24\sqrt{2}e^{-\sqrt{2}s(t)}, \tag{3.10}$$

where $v(\delta)$ is the solitary kink velocity. This expression is obtained in the ''dilute-defect gas approximation,'' that is, when the width of the fronts is much smaller than the distance between them. The first term in the right-hand of Eq. (3.10) can be either negative or positive and represents the contribution to the variation of the domain size owing to nonpotential effects. The second term is related to the interacting force between the kinks and it is always negative (attractive force) so that it tends to shrink the domain. If both terms are negative, the kinks will annihilate each other. Otherwise, when the first term is positive, the two effects act in opposite directions. In fact, given an initial size of the domain s_0, it is possible to find a value $\delta=\delta_c$ for which the domain neither shrinks nor grows; in this case, the initial domain would not evolve in time, being a stationary solution. For values $\delta>\delta_c$ the domain would get wider whereas for $\delta<\delta_c$ it would shrink. Note that in the $\delta=0$ case (potential regime), the isolated domain always collapses, but this can be stopped with a suitable strength of the nonpotential terms. Furthermore, given a fixed value of δ, if s_0 is large enough, the dominant term responsible for the kink motion is the one associated with $v(\delta)$. In this case the fronts move at a constant velocity leading to a variation of the domain size linear with time. On the other hand, if s_0 is small enough, kink interaction will be the dominant effect and the single domain size will collapse logarithmically with time. This picture of the size dynamics of a single domain also explains basically what happens when more domains (and a nonvanishing third amplitude) coexist. It gives a useful understanding of the characteristic growth laws obtained from a statistical analysis in the next section.

IV. DOMAIN GROWTH AND SCALING

In this section we focus on the scaling properties of the system (2.4) in a late stage of the dynamics, namely, when well-defined domains have formed. The scaling hypothesis

states that there exists a single characteristic length scale $R(t)$ such that the domain structure is, in a statistical sense, independent of time when lengths are scaled by $R(t)$. We will refer to the time dependence of the scale length as the *growth law* of the system. It has been found that the scaling hypothesis holds in a great variety of potential systems. The system under study here gives us the opportunity of answering the question of whether a nonpotential dynamics satisfies dynamical scaling.

Two magnitudes frequently used to study domain growth and scaling properties for a scalar field $\Psi(\mathbf{x},t)$ [for instance, one of the three amplitudes in Eq. (2.4)] are the equal time correlation function

$$C(\mathbf{r},t)=\left\langle \sum_{\mathbf{x}} \Psi(\mathbf{x}+\mathbf{r},t)\Psi(\mathbf{x},t)\right\rangle_{\text{i.c.}}, \tag{4.1}$$

and its Fourier transform, the equal time structure factor

$$S(\mathbf{k},t)=\left\langle \sum_{\mathbf{k}} \hat{\Psi}(\mathbf{k},t)\hat{\Psi}(-\mathbf{k},t)\right\rangle_{\text{i.c.}}, \tag{4.2}$$

where the angular brackets indicate an average over initial conditions (''runs''). If a single characteristic length exists, according to the scaling hypothesis, the pair correlation function and the structure factor must have the following scaling forms in a d-dimensional system:

$$C(\mathbf{r},t)=f(r/R(t)), \tag{4.3}$$

$$S(\mathbf{k},t)=R(t)^d\hat{f}(kR(t)). \tag{4.4}$$

The function f is called the *scaling function*. To check numerically the validity of the previous scaling laws, we have integrated the system of equations (2.4) using a finite difference method for both the spatial and temporal derivatives. In the simulations we have taken a constant value for η, namely, $\eta=3.5$, and we have varied δ from $\delta=0$ (potential case) to $\delta=0.1$ (a value below the Küppers-Lortz instability threshold). We have used periodic boundary conditions and have averaged our results over 100–500 runs. To study domain structure, we consider the correlation function of one of the three amplitudes. We use the correlation function better than the structure factor because of the large fluctuations of the structure factor at small wave numbers. A typical length scale associated with the average domain size can be defined in several ways. Specifically, we have determined it by computing the value of r for which $C(r,t)$ is half its value at the origin at time t, that is $C(R(t),t)=\frac{1}{2}C(0,t)$. The calculation has been performed by fitting the four points of $C(r,t)$ closest to $C(0,t)$ to a cubic polynomial. Another typical length, $R_1(t)$ can be evaluated directly as the system size divided by the number of kinks. We have verified that the quotient $R_1(t)/R(t)$ remains nearly constant, as expected, when a single characteristic length dominates the problem.

A. Growth law

We consider first the potential case $\delta=0$: in Fig. 5 we show that the domain size follows the expected logarithmic behavior. The attractive interaction among the kinks leads to a very long transient before the system reaches its final state, which corresponds to a one roll solution filling up the whole system.

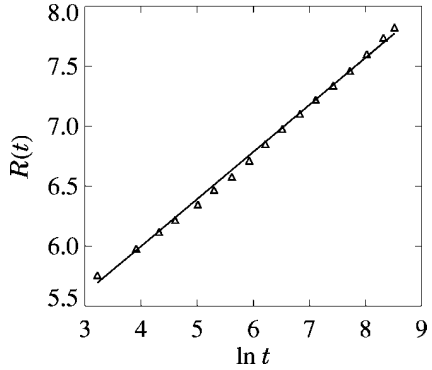

FIG. 5. Time evolution of the characteristic domain size for the potential case $\delta=0$ and $L=1000$. The straight line is a linear regression fit of points obtained numerically.

In the nonpotential case, the averaged domain size $R(t)$ is shown in Fig. 6 for a system of size 500 and $\delta=10^{-3}$. For the earliest times, when the kinks are very close to each other, and according to the discussion in Sec. III B, we expect the interaction terms to be the dominant ones (as long as δ is small enough). This leads to a logarithmic growth of $R(t)$ as observed in region I of Fig. 6. Due to coarsening the characteristic domain size becomes larger and the domain wall interaction becomes weaker as the time increases. For longer times the nonpotential effects dominate with respect to wall interaction. In this regime we can consider each domain wall to move at a constant velocity. We obtain for this stage a growth consistent with a linear profile with time (region III). Between regions I and III there exists a crossover (region II) for which the weights of both effects (interaction and nonpotential) in driving the domain wall motion are of the same order. Finally, at very late times finite size effects come into play (region IV): the domain size saturates to a constant value and the number of domain walls is too small to generate good statistics. When δ is large enough the initial kink annihilation is so fast that the regions I and II in the $R(t)$ plot can hardly be observed in the numerical integration. In this case of large nonpotential effects, a linear growth law is observed from the shortest times as shown in Fig. 7 for a very large system of size $L=100\,000$. For smaller systems finite size effects occur at relatively early times. For example, saturation effects appear for $t\gtrsim 200$ for a system of

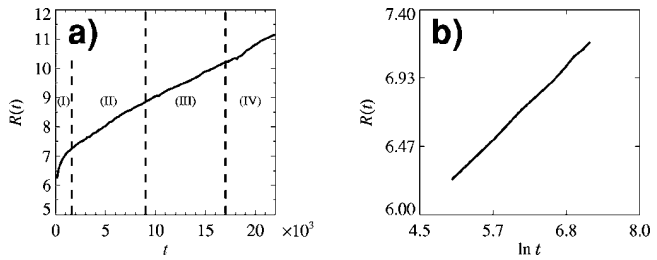

FIG. 6. (a) Time evolution of the characteristic domain size for $\delta=0.001$ and $L=1000$. The initial logarithmic growth law (region I) becomes linear (region III) after a crossover (region II). Region IV is related to finite size effects. (b) Closeup of region I in the left plot with logarithmic time scale.

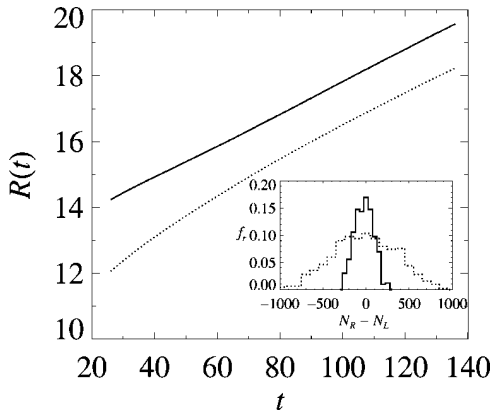

FIG. 7. Time evolution of the characteristic domain size for two distributions of the initial conditions with different width of the random variable $\Delta N = N_R - N_L$, which measures the difference between right and left moving interfaces. The inner plot shows the corresponding histograms in terms of the relative frequency of ΔN. The initial conditions were generated as explained in Sec. IV A. The growth exponents obtained numerically are close to 1.0 and 0.7 for the solid and dashed lines, respectively. Parameter values are $\eta = 3.5$ and $\delta = 0.1$; the system size is $L = 100\,000$.

size $L = 500$. The bigger δ, the sooner finite size effects appear.

In the regime for which the interaction effects are the dominant ones, we can give a simple explanation of the linear growth law observed based on mean field theory arguments. Statistically speaking, there will be the same number of kinks moving to the right and to the left. As a matter of fact, in an appropriate reference frame, the system can be seen as composed of motionless kinks (type 1) and kinks moving at a velocity of $2v$ in one fixed direction (type 2) . If we call $N_1(t)$ and $N_2(t)$ the *average* number of kinks of both types at time t, the number of kinks of, say type 1, at time $t+dt$ will be

$$N_1(t+dt) = N_1(t) - N_1(t) 2v\ dt \frac{N_2(t)}{L}, \qquad (4.5)$$

where the second term in the right-hand side represents the number of kinks disappeared in dt by annihilation and L stands for the system size. The important point is that $N_1(t) = N_2(t) = N(t)$ (remember we are dealing with averaged quantities), so that Eq. (4.5) transforms into $\dot{N}(t) = -(2v/L)N(t)^2$. The integration of the previous equation gives $N(t) = [(2v/L)t + N_0^{-1}]^{-1} \sim t^{-1}$, so that the average inter-kink distance $R(t) \sim N(t)^{-1} \sim t$ is linear with time.

We note that this mean field argument and the linear growth law does not hold for a discrete model with domain walls performing independent random walks; in this case a power law $R(t) \sim t^{1/2}$ can be rigorously demonstrated [24,32]. This fact is not surprising because it is known that growth laws for discrete and stochastic models may differ from those of the corresponding continuous and deterministic versions [33]. One representative example is the Ising model with Glauber dynamics versus the ϕ^4 model. In the former, the characteristic domain size grows as $R(t) \sim t^{1/2}$ [34] *independently of the dimensionality*, whereas in the latter the growth law is $R(t) \sim \ln t$ for $d = 1$ [20,21] and $R(t) \sim t^{1/2}$ for $d > 1$ [1,2]. An explanation for the failure of the mean field argument when applied to the discrete model is that the initial fluctuation ΔN in the number of kinks moving in each direction is important. It seems that such fluctuations are not significant enough in the continuous model in which domain walls emerge from a slight perturbation of the unstable state $A_1 = A_2 = A_3 = 0$. To check this idea we have computed the growth law $R(t)$ for the continuous system with modified initial conditions. We have generated initial conditions with a wider distribution of the random variable ΔN as follows: for each point x_j of the discretized mesh, a random number n_j from the set $\{1,2,3\}$ is chosen. Then the amplitude values at x_j are $A_k(x_j) = \delta_{kn_j}$, $k = 1,2,3$ (δ_{ij} stands for the Kronecker function). This generation of initial domain walls mimics the situation of a discrete model. The histogram of ΔN for the situations considered is shown in Fig. 7. For the artificially generated initial distribution of kinks we obtain a growth rate that is no longer linear as shown in Fig. 7.

We finally note that at long times the system will consist of a homogeneous roll state or a group of kinks moving either to the right or to the left [35]. Note that the periodic boundary conditions impose constraints on the number of such moving kinks. To be precise, the number of kinks moving in a fixed direction must be a multiple of three. We can form a subgroup of three kinks moving in the same direction by joining those appearing in each row of Fig. 2. The moving kinks will continue interacting among them until eventually they will all disappear. In this situation we expect the growth law to be logarithmic with time but one of such groups is composed typically of three, six, or rarely nine kinks, a number too small to generate good statistics.

B. Scaling function

We now address the question of the validity of the dynamical scaling hypothesis (4.3). For this purpose, we have plotted the equal time correlation function $C(r,t)$ versus the scaled length $r/R(t)$ for several times. Figure 8 shows the scaling function in the potential case. In Figs. 9 and 10 we show the correlation functions for several times before and after scaling the system length. Our results show that the correlation functions follow a single profile when the length is scaled with the characteristic domain sizes obtained above. We therefore conclude that a scaling description of the system is also valid as in the potential case, but now with a nonpotential dynamics. The upper limit of the time interval during which there is scaling is determined by the appearance of finite size effects. The range of values of δ for which there is scaling in a quite large time interval is rather small. For values of δ of even a few tenths, the finite size effects show up for very short times. Moreover the fluctuations in the scaling function grow as δ increases. For these reasons, we have not been able to obtain a conclusive comparison between scaling functions for different values of δ, although their shapes appear to be rather insensitive to the value of δ.

V. CONCLUSIONS

We have studied domain growth and dynamical scaling in a nonpotential coarsening process in one dimension. The

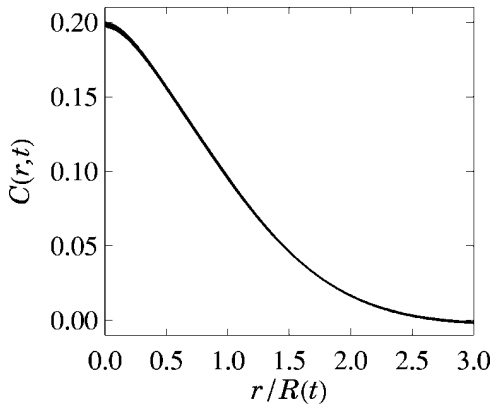

FIG. 8. Scaling function for the potential case $\delta=0$. The plot has been made by over plotting $C(r,t_i)$ vs $r/R(t_i)$ for several times from $t=200$ up to $t=5000$.

model considered features three coupled amplitudes. It is related to models of competing population species and to a three-mode description of the phenomenon of Rayleigh-Bénard convection in a rotating cell, although it cannot be used as a realistic model for this physical process. We have focused on the region below the Küppers-Lortz instability point, where the dynamics is still nonpotential and the system shows coarsening. A solitary kink moves at a constant velocity due to the nonpotential dynamics. When there are several kinks present in the system, these move due to both domain wall interaction and nonpotential effects. In any case the dynamics is governed by the motion of interfaces. This motion is such that kinks moving in opposite directions annihilate each other. As a consequence of kink annihilation the average domain size grows in time and the system coarsens. When $\delta=0$ (potential case) we have shown that, in accordance with general results, the growth law is logarithmic with time and that a scaling description of the system dynamics is possible. When δ becomes different from zero we have found that the scaling hypothesis still holds, as in the potential case, but with a different growth law that reflects the nonpotential dynamics of the system. For the shortest times, the kink interaction (the only effect present in the potential case) is the dominant effect and gives rise to a logarithmic growth law with time. For longer times the average interkink distance is large enough to make the interaction effects negligible in driving kink motion. Therefore each kink moves (at a constant velocity) nearly independently of the others as if it were isolated. This situation leads to a

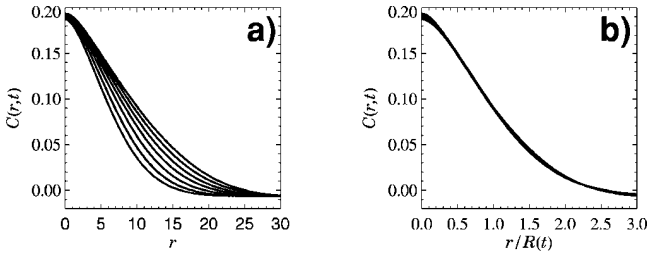

FIG. 9. (a) Equal time correlation function vs the nonscaled length for $\delta=0.001$, $L=1000$, and several different times from $t=150$ to $t=15\,000$. (b) Equal time correlation function vs the scaled length. The system parameters and the times for each curve are the same as in (a).

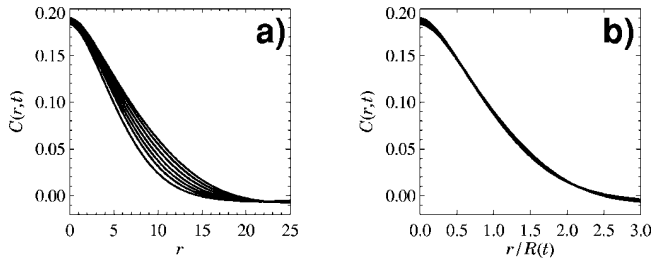

FIG. 10. (a) Equal time correlation function vs the nonscaled length for $\delta=0.1$, $L=1000$, and several different times from $t=15$ to $t=150$. (b) Equal time correlation function vs the scaled length. The system parameters and the times for each curve are the same as in (a).

growth law consistent with a linear profile with time. For larger values of δ the logarithmic region is not observed because of the fast annihilation of the domains during the very early times. The two dimensional version of this problem is currently under study [36] and it exhibits rather different dynamical behavior grossly dominated by vertices where three domain walls meet and which have no parallel in one dimensional systems.

ACKNOWLEDGMENTS

Financial support from DGYCIT (Spain) Projects Nos. PB94-1167 and PB94-1172 is acknowledged.

APPENDIX

We consider an isolated domain bounded by two domain walls associated with amplitudes A_1 and A_2, while $A_3=0$. When the domain size is much greater than the interface width (''dilute-defect gas approximation''), a reasonable *ansatz* for this solution is

$$\begin{aligned} A_1(x,t)&=a[x-r(t)]+b(x-d+r(t))+w_1(x,t),\\ A_2(x,t)&=b[x-r(t)]+a(x-d+r(t))-1+w_2(x,t), \end{aligned} \tag{A1}$$

where $r(t)$ measures the displacement of the kinks, d is the initial domain size [so that the domain size at time t is $d-2r(t)$], $\partial_t r$ and w_i $(i=1,2)$ are assumed to be small corrections of order δ and $\partial_t w_i$ to be negligible with respect to w_i. To simplify notation, we use $f\equiv f[x-r(t)]$, $f_d\equiv f[x-d+r(t)]$. The moving fronts a and b satisfy the boundary conditions $a(\infty)=b(-\infty)=0$, $a(-\infty)=b(\infty)=1$, and they are solutions of the system (2.4) (with one of the amplitudes equal to zero) so that the following equations hold:

$$\mathcal{M}_+(a,b)=\mathcal{M}_+(b_d,a_d)=\mathcal{M}_-(b,a)=\mathcal{M}_-(a_d,b_d)=0, \tag{A2}$$

where the action of the operators $\mathcal{M}_\pm(\cdot,\cdot)$ is given by

$$\mathcal{M}_\pm(f,g)=\partial_x^2\pm v(\delta)\partial_x+f-f^3-(\eta\pm\delta)fg^2. \tag{A3}$$

The parameter $v(\delta)$ is the front velocity as given by Eq. (3.9).

Introducing the ansatz (A1) into Eq. (2.4) we obtain, at leading order, a linear system of equations for w_1 and w_2:

$$\mathcal{L}\boldsymbol{\phi}=\boldsymbol{\phi}', \tag{A4}$$

$$\mathcal{L}=\begin{pmatrix} \partial_x^2+1-3(a+b_d)^2-\eta(b+a_d-1)^2 & -2\eta(a+b_d)(a_d+b-1) \\ -2\eta(a+b_d)(a_d+b-1) & \partial_x^2+1-3(a_d+b-1)^2-\eta(a+b_d)^2 \end{pmatrix},$$

$$\boldsymbol{\phi}=\begin{pmatrix} w_1 \\ w_2 \end{pmatrix}, \quad \boldsymbol{\phi}'=\begin{pmatrix} (\partial_x a+\partial_x b_d)v(\delta)+(\partial_x b_d-\partial_x a)\partial_t r+K_1\delta+K_2\eta+K_3 \\ (\partial_x b+\partial_x a_d)v(\delta)+(\partial_x a_d-\partial_x b)\partial_t r+K_1'\delta+K_2'\eta+K_3' \end{pmatrix},$$

where the functions $K_i(x,t)$ and $K_i'(x,t)$ $(i=1,2,3)$ are given by

$$K_1=a(a_d-1)^2+2b(a+b_d)(a_d-1)+b_d(1-2a_d+b^2),$$

$$K_2=a(a_d-1)^2+2(a_d-1)(ab+a_db_d+bb_d)+b_d(1+b^2),$$

$$K_3=-2\partial_x^2 b_d+b_d(3a^2+3ab_d+2b_d^2-2),$$

$$K_1'=-a(a+2b_d)(a_d-1)+b_d(b_d-2ab-bb_d),$$

$$K_2'=a(a+2b_d)(a_d-1)+b_d(2ab+bb_d+2a_db_d-b_d),$$

$$K_3'=-2\partial_x^2 a_d+3b^2(a_d-1)+3b(a_d-1)^2+2a_d^3-3a_d^2+a_d.$$

The solvability condition for the existence of a solution $(w_1(x,t),w_2(x,t))$ for Eq. (A4) reads

$$(\boldsymbol{\Psi}^\dagger,\ \boldsymbol{\phi}')=0, \tag{A5}$$

where $\boldsymbol{\Psi}^\dagger$ belongs to the kernel of the auto-adjoint linear differential operator $\mathcal{L}$. We will show below that $\boldsymbol{\Psi}^\dagger$ is approximately given by $(\partial_x a,\ \partial_x b)^T$ (here T denotes the transposed vector), where $a=a[x-r(t)]$ and $b=b[x-r(t)]$ are the domain wall profiles around $x=r(t)$.

The first component of the vector $\mathcal{L}\boldsymbol{\Psi}^\dagger$ is given by

$$(\mathcal{L}\boldsymbol{\Psi}^\dagger)_1=\mathcal{L}_{11}\partial_x a+\mathcal{L}_{12}\partial_x b=\partial_x^3 a+\partial_x a-3(a+b_d)^2\partial_x a - \eta(a_d+b-1)^2\partial_x a-2\eta(a+b_d)(a_d+b-1)\partial_x b. \tag{A6}$$

As long as that the width of the interfaces is much smaller than the domain size (for all times t), we can make the following approximations: $ab_d\approx 0$, $aa_d\approx a$, $bb_d\approx b_d$. Moreover, this assumption implies that the product of the derivative with respect to x of an amplitude solution centered on $x=x_0$ multiplied by another amplitude shifted a length of order of the domain size, will be a function that will take values different from zero only in a small region around $x=x_0$. By using the approximations

$$(a+b_d)^2\partial_x a\approx a^2\partial_x a,$$

$$(a_d+b-1)^2\partial_x a\approx b^2\partial_x a, \tag{A7}$$

$$(a+b_b)(a_d+b-1)\partial_x b\approx ab\partial_x b,$$

we find

$$(\mathcal{L}\boldsymbol{\Psi}^\dagger)_1=\partial_x[\partial_x^2 a+a-a^3-\eta b^2 a]. \tag{A8}$$

Taking the derivative of Eq. (2.4) with respect to x we find that the right-hand side of (A.8) is equal to zero when the amplitude solutions $a=a[x-r(t)]$ and $b=b[x-r(t)]$ are replaced by its form for $\delta=0$. Hence, we conclude that $(\mathcal{L}\boldsymbol{\Psi}^\dagger)_1=O(\delta)$. Likewise, we can prove that $(\mathcal{L}\Psi^\dagger)_2=O(\delta)$. Therefore, at lowest order in δ, $(\partial_x a,\ \partial_x b)^T$ belongs to the kernel of the operator $\mathcal{L}$.

Now we can calculate the evolution of the domain size $s(t)=d-2r(t)$ through the solvability condition (A5). We obtain

$$\partial_t s\cong\pm 2v(\delta)+\frac{\int_{-\infty}^{\infty}dx(h_a\partial_x a+h_b\partial_x b)}{\int_{-\infty}^{\infty}dx[(\partial_x a)^2+(\partial_x b)^2]} \tag{A9}$$

where the coefficients h_a and h_b depend upon the amplitude solutions a and b and the non-potential parameter δ. The first term of the right-hand side of Eq. (A9) represents the rate of change of the domain size due to nonpotential effects, which cause the kinks to move at a constant velocity $v(\delta)$. The second term is related to kink interaction. In the case $\eta=3$ we can compute explicitly all the coefficients involved in Eq. (A9) taking advantage of the analytical kink profiles at lowest order in δ [Eq. (3.3)]. Making an expansion in powers of $e^{-\sqrt{2}s(t)}$, retaining only the leading terms, and provided that δ is a small parameter, we obtain

$$\partial_t s=\pm\frac{\delta}{\sqrt{2}}-24\sqrt{2}e^{-\sqrt{2}s(t)}, \tag{A10}$$

which is Eq. (3.10).

[1] J. D. Gunton, M. San Miguel, and P. S. Sahni, in *Phase Transitions and Critical Phenomena*, edited by C. Domb and J. L. Lebowitz (Academic, London, 1983), Vol. 8.

[2] A. Bray, Adv. Phys. **43**, 357 (1994).

[3] P. C. Hohenberg and B. I. Halperin, Rev. Mod. Phys. **49**, 435 (1977).

[4] R. Montagne, E. Hernández-García, and M. San Miguel, Physica D **96**, 47 (1996).

[5] M. San Miguel and R. Toral, in *Instabilities and Nonequilibrium Structures VI*, edited by E. Tirapegui and W. Zeller (Kluwer Academic, Dordrecht, 1997), and references therein.
[6] M. C. Cross and D. I. Meiron, Phys. Rev. Lett. **75**, 2152 (1995).
[7] C. Josserand and S. Rica, Phys. Rev. Lett. **78**, 1215 (1997).
[8] L. Kramer, Z. Phys. B **41**, 357 (1981); **45**, 167 (1981).
[9] P. Coullet, J. Lega, B. Houchmanzadeh, and J. Lajzerowicz, Phys. Rev. Lett. **65**, 1352 (1990).
[10] P. Coullet, C. Elphick, and D. Repaux, Phys. Rev. Lett. **58**, 431 (1987).
[11] S. Fauve and O. Thual, Phys. Rev. Lett. **64**, 282 (1990).
[12] E. Meron, Phys. Rep. **218**, 1 (1992).
[13] D. J. Amit, in *Field Theory, The Renormalization Group and Critical Phenomena* (World Scientific, Singapore, 1984).
[14] Y. Hu, R. E. Ecke, and G. Ahlers, Phys. Rev. Lett. **74**, 5040 (1995); Phys. Rev. E **55**, 6928 (1997).
[15] G. Küppers and D. Lortz, J. Fluid Mech. **35**, 609 (1969).
[16] F. H. Busse and K. E. Heikes, Science **208**, 173 (1980).
[17] Y. Tu and M. C. Cross, Phys. Rev. Lett. **69**, 2515 (1992).
[18] M. C. Cross, D. Meiron, and Y. Tu, Chaos **4**, 607 (1994).
[19] A. J. Bray, B. Derrida, and C. Godreche, Europhys. Lett. **27**, 175 (1994).
[20] A. D. Rutenberg and A. D. Bray, Phys. Rev. E **50**, 1900 (1994).
[21] T. Nagai and K. Kawasaki, Physica A **134**, 483 (1986).
[22] F. de Pasquale, P. Tartaglia, and P. Tombesi, Physica A **31**, 2447 (1985).
[23] K. Kawasaki and T. Ohta, Physica A **116**, 573 (1982).
[24] L. Frachebourg, P. L. Krapivsky, and E. Ben-Naim, Phys. Rev. E **54**, 6186 (1996).
[25] R. M. May and W. J. Leonard, SIAM (Soc. Ind. Appl. Math.) J. Appl. Math. **29**, 243 (1975).
[26] R. Toral and M. San Miguel (unpublished).
[27] A. C. Newell and J. A. Whitehead, J. Fluid Mech. **38**, 279 (1969).
[28] L. A. Segel, J. Fluid Mech. **38**, 279 (1969).
[29] G. H. Gunaratne, Q. Ouyang, and H. L. Swinney, Phys. Rev. E **50**, 2802 (1994).
[30] S.-K. Chan, J. Chem. Phys. **67**, 5755 (1977).
[31] B. A. Malomed, A. A. Nepomnyashchy, and M. I. Tribelsky, Phys. Rev. A **42**, 7244 (1990).
[32] Y. Elskens and H. L. Frisch, Phys. Rev. A **31**, 3812 (1985).
[33] S. N. Majumdar and D. A. Huse, Phys. Rev. E **52**, 270 (1995).
[34] A. J. Bray, J. Phys. A **22**, L67 (1989).
[35] We have checked on our numerical simulations, that on average, half the runs lead to a state corresponding to a group of kinks moving to the right and half of them to kinks moving to the left.
[36] R. Gallego, M. San Miguel, and R. Toral (unpublished).